### C. Final Result

Substituting in the result of (23) into the original simplified expression of (20), the trace of the matrix product $R_1 R_2^{-1}$, where both $R_1$ and $R_2$ are symmetric Toeplitz matrices, is expressed as

$$tr[R_1 R_2^{-1}] = r_1(0)\sum_{i=1}^{N} u_2(i,i) + 2\sum_{j=1}^{N} r_1(j) \sum_{i=0}^{N-j} u_2(i+j,i)$$
$$= r_1(0)\hat{r}_a(0) + 2\sum_{j=1}^{N} r_1(j)\hat{r}_a(j). \quad (24)$$

## REFERENCES


[1] S. Kullback, *Information Theory and Statistics*. New York: Dover, 1968.

[2] I. Csiszar, "I-divergence geometry of probability distributions and minimization problems," *Ann. Prob.*, vol. 3, pp. 146–158, 1975.

[3] T. Kailath, "The divegence and Bhattacharyya distance measures in signal detection," *IEEE Trans. Comm. Tech.*, vol. COM-15, pp. 52–60, Feb. 1967.

[4] R. Johnson, "Axiomatic characterization of the directed divergences and their linear combinations," *IEEE Trans. Inform. Theory*, vol. IT-25, pp. 709–716, Nov. 1979.

[5] Y. Linde, A. Buzo, and R. Gray, "An algorithm for vector quantization design," *IEEE Trans. Commun.*, vol. COM-28, pp. 84–95, Jan. 1980.

[6] J. Shore, "Minimum cross-entropy spectral analysis," *IEEE Trans. Acoust. Speech Signal Processing*, vol. ASSP-29, pp. 230–237, Apr. 1981.

[7] R. Gray, A. Buzo, A. Gray, Jr., and Y. Matsuyama, "Distortion measures for speech processing," *IEEE Trans. Acoust. Speech Signal Processing*, vol. ASSP-28, pp. 367–376, Aug. 1980.

[8] W. Gersch, F. Martinelli, J. Yonemoto, M. Low, and J. McEwan, "Automatic classification of electroencephalograms: Kullback-Leibler nearest neighbor rules," *Sci.*, vol. 34, pp. 193–195, July 1979.

[9] F. Itakura and S. Saito, "An analysis-synthesis telephony based on maximum likelihood method," in *Proc. Int. Cong. Acoust.*, 1968, vol. C-5-5, pp. C17-20.

[10] R. Gray, A. Gray, Jr., G. Rebolledo, and J. Shore, "Rate-distortion speech coding with a minimum discrimination information distortion measure," *IEEE Trans. Inform. Theory*, vol. IT-27, pp. 708–721, Nov. 1981.

[11] A. H. Gray, Jr. and J. D. Markel, "Distance measures for speech processing," *IEEE Trans Acoust. Speech Signal Processing*, vol. ASSP-24, pp. 380–391, Oct. 1976

[12] G. Golub and C. Van Loan, *Matrix Computations*. Baltimore, MD: John Hopkins University Press, 1983.

[13] S. Marple, Jr., *Digital Spectral Analysis with Applications*. Englewood Cliffs, NJ: Prentice-Hall, 1987.

[14] S. Levinson, L. Rabiner, A. Rosenberg, and J. Wilson, "Interactive clustering techniques for selecting speaker-independent reference templates for isolated word recognition," *IEEE Trans. Commun.*, vol. COM-28, pp. 84–95, Jan. 1980.


# Building a Sonar Map in a Specular Environment Using a Single Mobile Sensor

Ömür Bozma and Roman Kuc

*Abstract*— **The physical properties of acoustic sensors are exploited to obtain information about the environment for sonar map building. A theoretical formulation is presented for interpreting the sensor data based on the physical principles of acoustic propagation and reflection. A novel characterization of the sonar scan is described that allows the differentiation of planes, corners, and edges in a specular environment. A single sensor mounted on an autonomous vehicle in our laboratory verifies the technique. The implication to sonar map building and the limitations of differentiating elements with one sensor are discussed.**

## I. INTRODUCTION

Acoustic sensors have been widely used for determining the proximity of objects and have been employed for robot navigation and map building [1]–[6]. *Time-of-flight* (TOF) systems similar to that implemented by Polaroid [7] provide a convenient and a low-cost way for range measurements using acoustic sensors [5], [8]–[10]. Reliable sonar map building and navigation requires a thorough characterization and interpretation of the sensor data. Although more researchers [11], [12] are realizing the importance of the physical principles in implementing more robust sonar systems, there has not been much work in this area. The contribution of this paper is to exploit the physical principles of reflection to interpret sensor data in a specular environment. With such an approach, better and more reliable sonar maps of the environment can be constructed.

Most research with acoustic sensors has been conducted assuming a rough environment for which echoes are received for most look directions [2], [6], [13], [14]. Reflections from specular surfaces have usually been treated as artifacts, although many surfaces in the real world behave as specular reflectors. Physical properties of specular surfaces have been studied to interpret their sonar reflections [15]–[19]. A recent paper [20] provides a general model of reflections from surfaces with varying degrees of roughness.

In this paper, a new concept is introduced for interpreting sonar TOF data obtained from specular surfaces using a single mobile sensor for generating sonar maps. A parameterization of the arc formed when the sensor scans across an object is developed. These parameter values are then used to differentiate the elements in the environment. The procedure is then verified by a single sensor mounted on an autonomous vehicle in our laboratory.

The paper is organized in the following manner: Section II describes the acoustic sensor. A model of the environment consisting of planes, corners, and edges is presented in Section III. A parametric characterization of the scan that allows the differentiation of objects is developed in Section IV. The differentiation algorithm is presented in Section V. Constraints on the translation of the autonomous vehicle is given in Section VI. Verification of the theory for differentiation of objects using a mobile vehicle is presented in Section VII. Finally, the necessary conditions for successful differentiation and interference effects are described in Section VIII.

Manuscript received March 28, 1989; revised June 17, 1991. This work was supported by the National Sciene Foundation under grants ECS-8611801 and ECS-8802627. Recommended for acceptance by O. Faugeras.

The authors are with the Intelligent Sensors Laboratory, Department of Electrical Engineering, Yale University, New Haven, CT 06520.

IEEE Log Number 9104536.

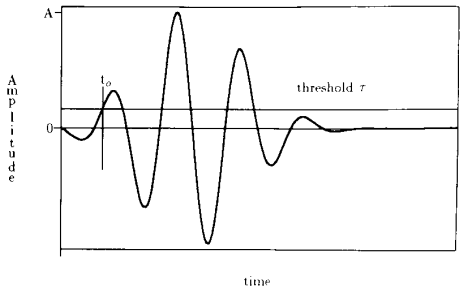


Fig. 1. Typical echo of the ultrasound ranging system.

## II. The Acoustic Sensor

The acoustic sensor in the pulse/echo mode acts as both a transmitter and a receiver. A voltage pulse first excites the transmitter, which causes an acoustic pulse to be emitted. The echo reflected from an object may be detected by the same sensor now acting as a receiver. A typical echo observed at the output of the sensor having maximum amplitude $A$ is shown in Fig. 1. A conventional TOF system produces a range value when the echo amplitude first exceeds the *threshold level* $\tau$, which is shown to occur at time $t_o$. A range measurement $r_o$ is obtained from the round-trip TOF by

$$r_o = \frac{ct_o}{2} \tag{1}$$

where $c$ is the speed of sound in air (343 m/s at 20° [21]), and $t = 0$ corresponds to the transmit time.

The transmitting sensor forms a directed beam, which contains the propagating pulse. A plane piston of radius $a$ enclosed in an infinitely large baffle and vibrating at frequency $f_R$ is commonly used to model the transmitter [22]. The beam pattern then consists of two distinct regions: 1) the *near (Fresnel) zone*, in which the beam is contained within a cylinder and 2) the *far (Fraunhofer) zone*, in which the beam diverges. One measure of the angular beam width in the far zone is the half-width beam angle $\theta_o$, which is given by

$$\theta_o = \sin^{-1}\left(\frac{0.61\,\lambda}{a}\right) \tag{2}$$

where $\lambda = \frac{c}{f_R}$ is the wavelength of the acoustic signal, and $a$ is the aperture radius. The start of the far zone is usually taken as $r_f = a^2/\lambda$ [23]. For the Polaroid sensor $f_R = 60$ kHz, $\lambda = 5.7$ mm, $a = 1.7$ cm, $\theta_o = 11.8°$, and $r_f = 5$ cm. The $a$ is the effective radius of the transducer, as measured between the outermost grooves on the transducer plate (see p. 4/11 of [7]). The far-zone characteristics are used in developing the techniques to analyze the environment since most of the reflectors will be in that region.

For single-frequency excitation, the beam pattern has the shape described by a Bessel function (see p. 227 of [24]). In the pulse mode, the beam pattern becomes increasingly Gaussian as more frequencies are introduced in the broad-band pulse. If the sensor line-of-sight is defined by $\theta = \alpha$, the maximum pulse amplitude at distance $r$ and deviation $\theta$ can be modeled in the far zone by [25]

$$A(r,\theta) = \frac{A_f r_f}{r} e^{-2(\theta-\alpha)^2/\theta_o^2} \tag{3}$$

where $A_f$ is the amplitude at range $r_f$ along the sensor line of sight.

The next section describes the environment and the structures that produce echoes in this environment.

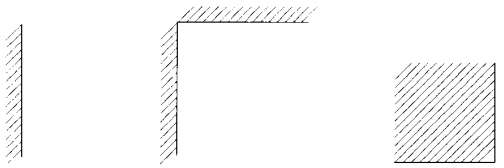

Fig. 2. Plane, corner, and edge as seen in the 2-D floor plan.

## III. Model of the Environment

The environment considered in this paper consists of *specular* (mirror-like) surfaces. A surface is specular if its roughness is much smaller than the incident wavelength. Since the 60-kHz Polaroid sensor has a wavelength of 5.7 mm, many surfaces encountered in the real world can be considered to be specular. To describe the locations and orientations of objects lying in space, two coordinate frames are defined [26]:

1) a *world coordinate* system, whose origin coincides with the initial position and orientation of the vehicle
2) a *base frame*, in which positions and orientations are given with respect to the base of the sensor (or vehicle).

The $x$ and $y$ axes are chosen to lie on the horizontal plane, and the $z$ axes in both frames are chosen along the vertical direction. Although measurements are usually made with respect to the base frame, world coordinates allow the location and orientation of the vehicle with respect to the initial position to be tracked, and the spatial relation of the objects identified can be determined to generate a sonar map.

The elements in this world are classified as planes, corners, and edges. We first define an *extension* of a curve in a given direction as the surface that is generated by translating the curve along that direction. All the elements are extensions in the $z$ direction of 2-D objects. A *plane* is the extension of a line segment lying on the $x$-$y$ plane. A *corner* is the intersection of two planes as observed from inside the convex space generated. An *edge* is the intersection of two planes as observed from inside the concave space generated. Fig. 2 shows the plane, corner, and edge elements as seen in the 2-D floor plan. Right-angle corners and edges are used in our model since they are encountered most frequently in the real world. The echoes obtained from the three elements are now examined in more detail in the next section.

### A. Planes and Corners

For plane and corner reflectors, the incident beam is redirected with the angle of reflection being equal to the angle of incidence. Such reflectors can be treated as mirrors, and the transmitter/receiver (T/R) can be broken up into a separate transmitter (T) and a virtual receiver (R'), as shown in Fig. 3 [15]. For the detection of the echo to occur, part of this redirected beam must fall on the receiver aperture and produce a signal whose amplitude exceeds the threshold level $\tau$. Breaking up the sensor in this fashion clearly shows that only the pulse transmitted in the direction normal to the reflecting surface is detectable by the receiver. As the sensor scans across the object, an arc is formed from TOF dots since the range is measured from the normal incidence on the object while the dots are placed along the sensor line of sight. The arcs formed by scanning across a plane and a corner are shown in Fig. 4. Since the resulting arcs are identical, it is impossible to differentiate a plane from a corner on the basis of the information obtained only from one scan [15].

However, it is possible to differentiate planes and corners using a single sensor when the sensor is allowed to move. A parametric

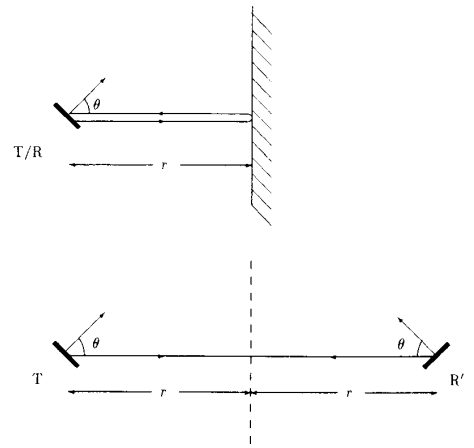


Fig. 3. Separation of transmitter/receiver (T/R) into separate transmitter (T) and receiver (R') for a plane reflector. For a corner, the orientation of the virtual receiver is reversed [16].

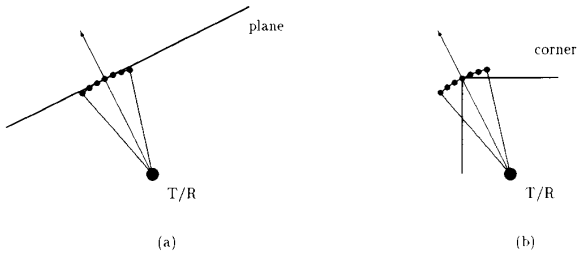


Fig. 4. Arc formed by (a) a plane and (b) a corner. Identical arcs are produced by both elements.

description of the arcs formed by the scans based on both the reflecting properties of the surfaces and the sensor is necessary to develop a procedure to accomplish this differentiation.

According to (3), the amplitude of the transmitted pulse decreases with range in the far zone since the diameter of the beam cross section increases with range with divergence angle $2\theta_o$. A time-controlled amplifier, whose gain increases with range, has been included to compensate for this spreading loss, as well as the attenuation of sound in air [7], [21]. Then, the amplitude of the echo from a plane or a corner becomes independent of range. As the sensor scans across a plane or corner reflector, the echo amplitude follows the Gaussian curve shown in Fig. 5 and given by

$$A_{PC}(\theta) = A_f\, e^{-4(\theta-\theta_N)^2/\theta_o^2} \quad \text{for } r > r_f \tag{4}$$

where $\theta_N$ denotes the sensor orientation in the base frame that produces the echo with the maximum amplitude. For a plane, this occurs when the sensor orientation is normal to the surface and for the corner when the sensor points at the intersection of the planes that define the corner. The $\theta_N$ defined above has three important properties:

a) The maximum echo amplitude from an element occurs at $\theta = \theta_N$.
b) Due to symmetry of the sensor and the scanning procedure, the center of the scan arc occurs at $\theta = \theta_N$.
c) The location of the object is along the direction $\theta = \theta_N$.

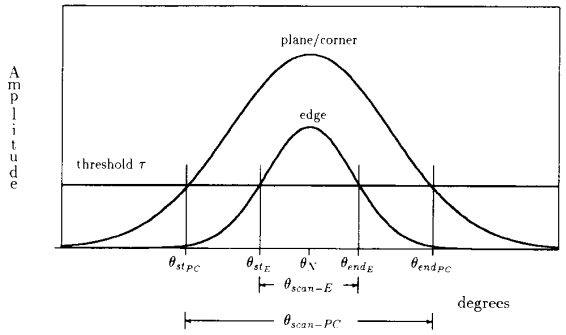


Fig. 5. Amplitude of the echo versus the orientation of the sensor. For edges, the amplitude is also a function of the range. For all ranges, the amplitude of the echo obtained from a planes or a corner is always greater than that from an edge.

Let the sensor perform a scan and denote the minimum and maximum angles of sensor orientations for which the echo amplitude exceeds the threshold by $\theta_{st_{PC}}$ and $\theta_{end_{PC}}$. Hence, the reflectors are detected only when $\theta_{st_{PC}} \leq \theta \leq \theta_{end_{PC}}$, as shown in Fig. 5.

Using these physical and geometrical results, isolated planes and corners can be differentiated by scanning from two different locations. To illustrate this, let the scan from location I produce an arc centered at $p_1 = (x_1, y_1)$, as shown in Fig. 6. Let $\theta_{N_I}$ be the orientation of the object from I in the base frame, as determined from the center of the arc formed. Let us now translate the sensor from location I to II and perform a second scan. Since a right-angle corner reflects an echo back to the sensor, independent of the sensor location, the scan from II for a corner still produces an arc centered at $p_1 = (x_1, y_1)$. However, the arc has a different orientation, denoted by $\theta_{N_{II}}$, as seen in Fig. 6(a). For any given translation length, to maximize the orientation difference of a corner as seen from two locations, the direction of travel from I to II should be chosen at angle $\gamma = \pm \arccos\left(\frac{\Delta}{r_I}\right)$ from $\theta_{N_I}$, where $\Delta$ is the translation length, and $r_I$ is the distance to the corner from I. As seen in Fig. 6, the orientation difference is maximized when the line from the corner to II is tangent to the circle centered at I with radius $\Delta$.

For the plane, however, the scan from II produces an arc centered at $p_2 = (x_2, y_2)$, which is tangential to the plane at another point. In this case, $\theta_{N_I} = \theta_{N_{II}}$, as shown in Fig. 6(b), indicating that the arcs formed for a plane preserve the same orientation independent of the direction of movement.

The basis for differentiating planes and corners is the angular difference between $\theta_{N_I}$ and $\theta_{N_{II}}$. For a plane $\theta_{N_I} - \theta_{N_{II}} = 0$, whereas for a corner $\theta_{N_I} - \theta_{N_{II}} \neq 0$. The translation length $\Delta$ plays an important role in the differentiation process and is analyzed in more detail in Section VI.

### B. Edges

When the transmitted pulse encounters an element having dimensions less than $\lambda$, a *diffracted* echo results. The diffracted echo from the edge is characterized by a cylindrically diverging wave that appears to be emanated from the line defining the edge. The decrease in the amplitude of this cylindrical wave is proportional to the inverse square root of the distance traveled [15], [27], [28]. The smallest diffracted echo produced in our environment is by the edge. The amplitude of the detected echo from an edge, as a scan is performed, is approximated by the curve shown in Fig. 5 and given

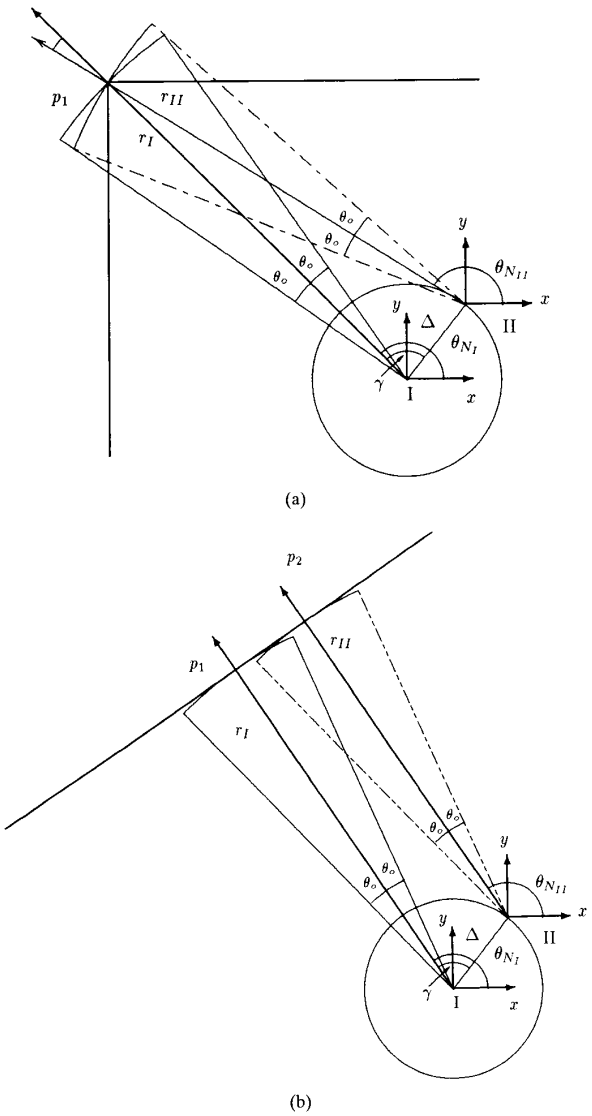


Fig. 6. (a) Illustration of the differentiation procedure for the corner. The centers of the arcs coincide, but they have different orientations $(\theta_{N_I} \neq \theta_{N_{II}})$; (b) illustration of the differentiation procedure for the plane. The centers of the arcs separate, but the orientations stay the same: $(\theta_{N_I} = \theta_{N_{II}})$.

by [16]

$$A_E(\theta, r) = \sigma_E \frac{A_f r_f^{1/2}}{r^{1/2}} e^{-4(\theta-\theta_N)^2/\theta_o^2} \quad \text{for } r > r_f \tag{5}$$

where $\sigma_E$ is the scattering strength [29] that depends on the sharpness of the edge and varies with the orientation of the edge. For a 90° edge and the 60-kHz Polaroid sensor, $\sigma_E$ was empirically found to vary between 0.035 and 0.10. The maximum echo amplitude results at $\theta = \theta_N$ when the sensor is oriented at the line defining the edge. Note that $\theta_N$ in (5) has the same properties given in Section III-A.

Given the echo characteristics of planes/corners and edges as defined in (4) and (5), respectively, the echo amplitude from planes and corners is always greater than that of edges in the far field for the 60-kHz Polaroid sensor, that is

$$A_{PC}(\theta) > A_E(\theta, r) \qquad \text{for } r > r_f. \tag{6}$$

This result can also be explained in radar terms, where the edge is said to have a smaller *scattering cross section* than that of a flat surface [30].

From (5), it is seen that for any given threshold $\tau$, there exists a range $r_{\max_E}$ beyond which an edge cannot be detected, given by

$$r_{\max_E} = \left(\frac{\sigma_E A_f}{\tau}\right)^2 r_f. \tag{7}$$

This maximum range of detection for an edge occurs when the threshold $\tau$ just equals the echo amplitude, and the sensor is looking straight at the edge at $\theta = \theta_N$.

These physical properties of edges will now be exploited to develop a parameterization that will enable us to differentiate edges from planes and corners. Let $\theta_{st_E}$ and $\theta_{end_E}$ denote the minimum and maximum angles of sensor orientation, respectively, in the base frame, for which the echo amplitude from an edge exceeds the threshold level. As seen in Fig. 5, an edge can be detected only when the sensor orientation $\theta$ lies in the interval $[\theta_{st_E}, \theta_{end_E}]$. We define the *angular extent* $\theta_{scan}$ of an element as the range of angles for which detection occurs. Let $\theta_{scan_{PC}}$ and $\theta_{scan_E}$ denote the angular extent of planes/corners and edges, respectively

$$\begin{aligned} \theta_{scan_{PC}} &= \theta_{end_{PC}} - \theta_{st_{PC}}. \\ \theta_{scan_E} &= \theta_{end_E} - \theta_{st_E}. \end{aligned} \tag{8}$$

Since the echo obtained from edges is weaker than that obtained from planes and corners, the angular extent of edges is smaller than that of planes and corners, or

$$\theta_{scan_E} < \theta_{scan_{PC}}. \tag{9}$$

The next section describes the formation of the scan, which is the key to the differentiation procedure.

## IV. Formation of the Scan

In practice, the scan is usually performed in discrete rotational steps. This quantization introduces random errors in the measurement of the scan extent and orientation. Additive noise in the observed waveforms will be assumed to be negligible to simplify the analysis. Let us consider a counterclockwise rotation of the sensor in performing a scan, with incremental angle of rotation of the sensor $\delta\theta$. The $i$th angle of rotation is then given by

$$\theta_i = i\ \delta\theta.$$

Let $\theta_{st}$ and $\theta_{end}$ denote the minimum and maximum angles for which the echo amplitude exceeds the threshold $\tau$. Because of the quantization in the angles of rotation, $\theta_{st}$ and $\theta_{end}$ cannot be determined exactly. The measured values $\hat{\theta}_{st}$ and $\hat{\theta}_{end}$ are therefore estimates of their true values, as shown in Fig. 7.

Due to the symmetry of the scan, the true value of $\theta_N$ is given by

$$\theta_N = \frac{\theta_{st} + \theta_{end}}{2}.$$

Hence, a reasonable estimate for $\theta_N$, denoted by $\hat{\theta}_N$, is given by

$$\hat{\theta}_N = \frac{\hat{\theta}_{st} + \hat{\theta}_{end}}{2}. \tag{10}$$

A counterclockwise scan corresponds in Fig. 7 to proceeding from left to right in $\theta$. Let $\theta_1$ and $\theta_2$ be the observed minimum and maximum sensor orientations in the base frame, respectively, for

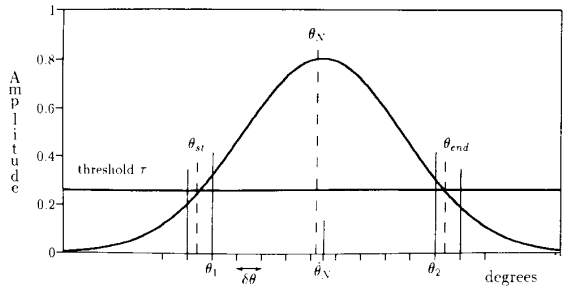


Fig. 7. Amplitude of the echo versus the sensor orientation with discrete angles of rotation. The true and estimated values for the different angular parameters are shown.

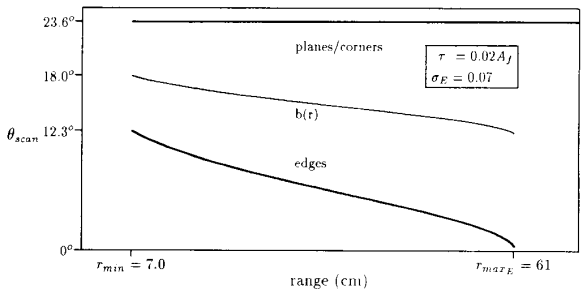


Fig. 8. Comparison of the true values of the angular extents of planes and corners with edges for the 60-kHz Polaroid sensor. The angular extent of edges is always less than that of planes and corners. The curve $b(r)$ shows the boundary for differentiation.

which the echo amplitude exceeds the threshold $\tau$. To account for the quantization, let us define

$$\hat{\theta}_{st} = \theta_1 - \frac{\delta\theta}{2}$$
$$\hat{\theta}_{end} = \theta_2 + \frac{\delta\theta}{2}. \tag{11}$$

In terms of the true values, we have

$$\hat{\theta}_{st} = \theta_{st} + \epsilon_{st} - \frac{\delta\theta}{2}$$
$$\hat{\theta}_{end} = \theta_{end} - \epsilon_{end} + \frac{\delta\theta}{2} \quad , \quad \epsilon_{st}, \epsilon_{end} > 0 \tag{12}$$

where $\epsilon_{st}$ and $\epsilon_{end}$ are independent random variables that are uniformly distributed between 0 and $\delta\theta$. From (10) and (12), we obtain

$$\hat{\theta}_N = \theta_N + \frac{\epsilon_{st} - \epsilon_{end}}{2}.$$

By taking the expected value of this estimate, we find

$$E\{\hat{\theta}_N\} = \theta_N,$$

where $E\cdot$ is the expected value operator [31]. Hence, $\hat{\theta}_N$ is an unbiased estimator.

In a similar fashion, the estimate of the angular extent $\hat{\theta}_{scan}$ is given by

$$\hat{\theta}_{scan} = \hat{\theta}_{end} - \hat{\theta}_{st}. \tag{13}$$

Using (12), we find

$$\hat{\theta}_{scan} = \theta_{scan} + \delta\theta - (\epsilon_{st} + \epsilon_{end}). \tag{14}$$

The expected value of the estimate of the angular extent is as follows:

$$E\{\hat{\theta}_{scan}\} = E\{\theta_{scan} + \delta\theta - (\epsilon_{st} + \epsilon_{end})$$
$$= \theta_{scan}$$

Thus, $\hat{\theta}_{scan}$ is also an unbiased estimator.

Planes, corners, and edges are differentiated on the basis of the orientation difference and angular extent of the scan arcs as shown in the next section.

## V. The Differentiation Procedure

### A. Differentiating Edges and Planes/Corners

The angular extent plays the key role in differentiating edges from planes and corners. From (9), it is noted that edges can be recognized by the size of their angular extent.

The true values of the angular extents of planes/corners and edges can be determined from (4) and (5). The extent of the scan of a plane or a corner is equal to the range of $\theta$ for which

$$A_{PC}(\theta) = A_f\, e^{-4(\theta-\theta_N)^2/\theta_o^2} \geq \tau.$$

From the definitions of $\theta_{st}$, $\theta_{end}$, and (9), we get

$$\theta_{scan_{PC}} = \theta_o \left[\ln\left(\frac{A_f}{\tau}\right)\right]^{1/2}. \tag{15}$$

Similarly, for $\theta_{scan_E}$, we get

$$\theta_{scan_E}(r) = \theta_o \left[\ln\left(\sigma_E \frac{A_f r_f^{1/2}}{\tau\ r^{1/2}}\right)\right]^{1/2}. \tag{16}$$

Note that for edges, the angular extent is also dependent on the range. Fig. 8 shows the plot of $\theta_{scan}$ as a function of range for the Polaroid sensor. Let $b(r)$ define a boundary between the true values of the angular extents for edges and planes/corners, as given by

$$b(r) = \frac{\theta_{scan_E}(r) + \theta_{scan_{PC}}}{2}. \tag{17}$$

The value of the angular extent is estimated with $\hat{\theta}_{scan}$ from (11) and (13). The differentiation can then be based on the following scheme:

$$\text{if } \hat{\theta}_{scan}(r) > b(r) \Longrightarrow \text{element is plane/corner}$$
$$\text{if } \hat{\theta}_{scan}(r) < b(r) \Longrightarrow \text{element is an edge} \tag{18}$$

where the success of differentiating edges from planes and corners can be determined from the probability density function (pdf) of $\hat{\theta}_{scan}$ denoted by $f_{\hat{\theta}_{scan}}(\hat{\theta}_{scan})$. In the noiseless case, the only random variable in the scan operation is the quantization error. Using the result of the sum of two random variables ($\epsilon_{st}$ and $\epsilon_{end}$) [31], we find

$$f_{\hat{\theta}_{scan}}(\hat{\theta}_{scan}) = \begin{cases} -\frac{|\hat{\theta}_{scan}-\theta_{scan}|}{\delta\theta^2} + \frac{1}{\delta\theta} & \text{for } |\hat{\theta}_{scan} - \theta_{scan}| < \delta\theta \\ 0 & \text{otherwise.} \end{cases} \tag{19}$$

This pdf, shown in Fig. 9(a), has a finite extent equal to $2\delta\theta$. Since $\theta_{scan_E} < \theta_{scan_{PC}}$, if the step size $\delta\theta$ is chosen sufficiently small, the pdf's for edges and planes/corners can be made to be nonoverlapping, implying perfect differentiation can be performed. From Fig. 9(b), this requires that $\theta_{scan_E} + \delta\theta < \theta_{scan_{PC}} - \delta\theta$. Thus, a necessary condition for differentiation edges from planes and corners with 100% accuracy is

$$\delta\theta < \frac{\theta_{scan_{PC}} - \theta_{scan_E}}{2} \tag{20}$$

where $\theta_{scan_{PC}}$ and $\theta_{scan_E}$ are as given in (15) and (16), respectively.

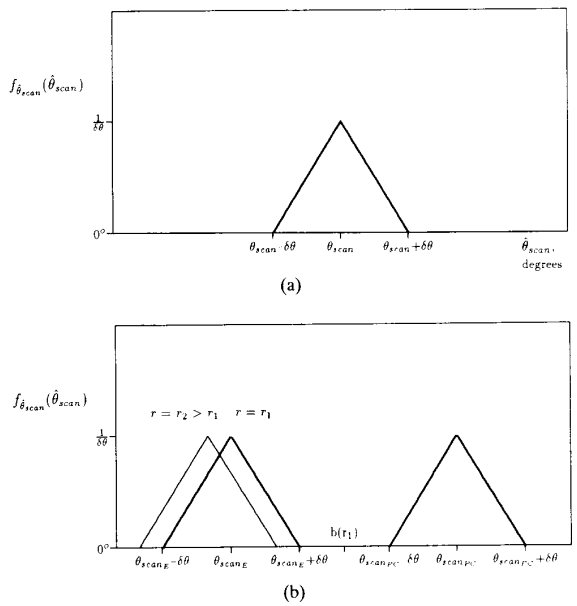


Fig. 9. (a) pdf of the angular extent estimate. The pdf has a finite spread of $(-\delta\theta, \delta\theta)$ around the mean value. For edges, the mean value is a function of range $r$; (b) pdf's of the angular extent estimates for edges and planes/corners. For successfully differentiating edges from planes and corners, the two pdf's must be nonoverlapping.

If an edge is detected, no further computation is needed. However, if the detected element is either a plane or a corner, further differentiation is necessary. This latter case is discussed below.

### B. Differentiating Planes and Corners

A single mobile sensor scanning a reflector from two positions is sufficient to perform the differentiation. The parameters to be estimated from the two scans are the orientation $\theta_{N_I}$ of the center of arc from position I, the orientation $\theta_{N_{II}}$ of the center of arc from position II, and distance $r_I$ to the element from position I. Estimates of $\theta_{N_I}$ and $\theta_{N_{II}}$ are calculated according to (10).

When the sensor encounters a plane or a corner during a scan, it first estimates the orientation of the arc formed from position I, which is denoted by $\hat{\theta}_{N_I}$. Then, it translates a fixed distance $\Delta$ in the direction $\hat{\theta}_{N_I} + \gamma$, where $\gamma = \arccos\left(\frac{\Delta}{r_I}\right)$, to position II and estimates $\hat{\theta}_{N_{II}}$. The differentiation procedure is based on the difference between the two angles, denoted by $\hat{\beta}$, that is

$$\hat{\beta} = \hat{\theta}_{N_I} - \hat{\theta}_{N_{II}}. \tag{21}$$

If the mobile sensor translates from I to II with direction $\gamma = \arccos\left(\frac{\Delta}{r_I}\right)$, the true orientation differences $\beta_C$ and $\beta_P$ for corners and planes, respectively, are given by

$$\beta_C = \arcsin\left(\frac{\Delta}{r_I}\right) \tag{22a}$$

$$\beta_P = 0. \tag{22b}$$

From the geometry of Fig. 6 and the definition of $\beta_C$, we get that $\sin\beta_C = \left(\frac{\Delta}{r_I}\right)$, yielding (22a). A similar analysis of Fig. 6(b) yields (22b).

The observed values $\hat{\beta}_P$ and $\hat{\beta}_C$ are computed from (21). The quantization of the rotation angles introduces an error and the success

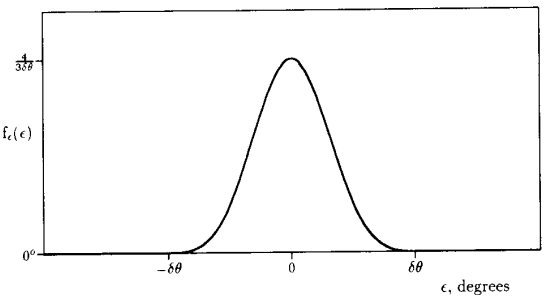


Fig. 10. pdf of $\epsilon$. The pdf of $\hat{\beta}$has a similar shape but a mean value of either $\beta_P$ or $\beta_C$, depending on whether the element being observed is a plane or a corner.

of differentiation can be determined from the pdf of $\hat{\beta}$. From (10), (12), and (21), we get

$$\hat{\beta} = \hat{\theta}_{N_I} - \hat{\theta}_{N_{II}} = \beta + \epsilon, \qquad \text{with } \epsilon = (\epsilon_{st_I} - \epsilon_{end_I} + \epsilon_{st_{II}} - \epsilon_{end_{II}})/2.$$

where subscripts $_{(I)}$ and $_{(II)}$ refer to positions I and II, respectively. The random variables $\epsilon_{st_I}, \epsilon_{end_I}, \epsilon_{st_{II}}$ and $\epsilon_{end_{II}}$ are assumed to be distributed uniformly in the interval $[0, \delta\theta]$ and are assumed to be mutually independent. Employing the methods for determining the pdf of the sum and difference of random variables [31], the pdf for $\epsilon$, denoted by $f_\epsilon(\epsilon)$, can be shown to be (Fig. 10)

$$f_\epsilon(\epsilon) = \begin{cases} \frac{8}{3\delta\theta^4}(\epsilon + \delta\theta)^3 & -\delta\theta \le \epsilon \le -\delta\theta/2 \\ \frac{4}{3\delta\theta^4}(-6\epsilon^3 - 6\epsilon^2\delta\theta + \delta\theta^3) & -\delta\theta/2 \le \epsilon \le 0 \\ \frac{4}{3\delta\theta^4}(6\epsilon^3 - 6\epsilon^2\delta\theta + \delta\theta^3) & 0 \le \epsilon \le \delta\theta/2 \\ \frac{8}{3\delta\theta^4}(-\epsilon + \delta\theta)^3 & \delta\theta/2 \le \epsilon \le \delta\theta \\ 0 & \text{otherwise.} \end{cases} \tag{23}$$

The pdf of $\hat{\beta}$, which is denoted by $f_{\hat{\beta}}(\hat{\beta})$, will be the same as $f_\epsilon(\epsilon)$, except that it will have a mean equal to $\beta$.

Since $f_{\hat{\beta}}(\hat{\beta})$ has a finite extent, which is equal to $2\delta\theta$, the elements can be differentiated correctly when $|\beta_C - \beta_P| > 2\delta\theta$. The mean value will either be $\beta_P$ or $\beta_C$, depending on whether the element scanned is a plane or a corner. Whenever $\hat{\beta}$ falls within $\pm\delta\theta$ of $\beta_P$, that element is considered to be a plane, and whenever it falls within $\pm\delta\theta$ of $\beta_C$, it is considered to be a corner, that is

$$\begin{aligned} &\text{if } |\hat{\beta} - \beta_P| \le \delta\theta \Longrightarrow \text{ element is a plane,} \\ &\text{if } |\hat{\beta} - \beta_C| \le \delta\theta \Longrightarrow \text{ element is a corner.} \end{aligned} \tag{24}$$

Having a procedure to differentiate planes, corners, and edges, the constraints on $\Delta$ are analyzed in the next section.

## VI. Constraints on Translation Length $\Delta$

As mentioned in Section III-A, the distance $\Delta$ plays a vital role in the differentiation process. If $\Delta$ is too small, the separation specified in (24) cannot be achieved with any statistical accuracy. On the other hand, a large $\Delta$ implies that the vehicle must travel a long distance, with possible echoes interfering from other objects or losing the previous element from its line of sight.

If the only source of error is due to the discrete rotation angles of the sensor, to differentiate between planes and corners successfully

$$\Delta \ge r_I \sin(2\delta\theta). \tag{25}$$

Then, the pdf's for planes and corners are nonoverlapping, as seen in Fig. 11(a). Since, the intervals $[-\delta\theta, \delta\theta]$ and $[\beta_C - \delta\theta, \beta_C + \delta\theta]$ must be nonoverlapping, we have $\beta_C > 2\delta\theta$. For $\frac{-\pi}{2} \le \beta_C \le \frac{\pi}{2}$ , $\sin\beta_C$

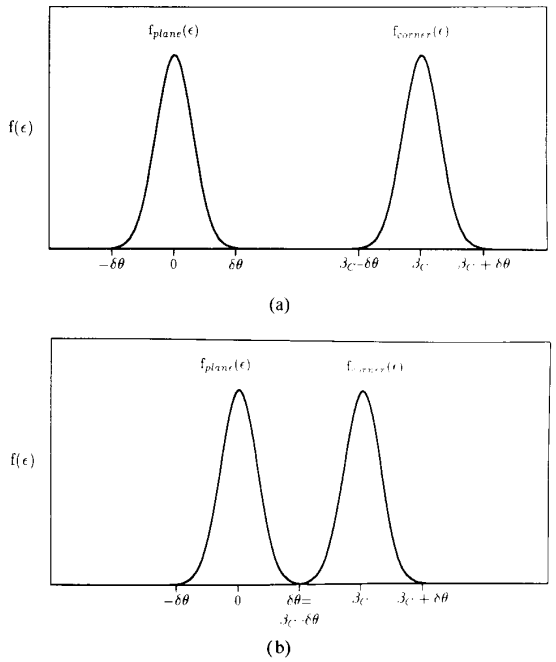


Fig. 11. (a) pdf of $\hat{\beta}$ shown both for plane and corner elements. $\beta_C$ is a function of the ratio of the translation length $\Delta$ and the range from the first location $r_1$. $\beta_C$ should be large enough so that the two pdf's do not intersect, i.e. $\beta_C \geq 2\delta\theta$; (b) pdf of $\hat{\beta}$ shown with the translation length $\Delta_{\min}$ satisfying the lower bound condition $\Delta_{\min} = r_1 \sin(2\delta\theta)$.

is an increasing function such that $\beta_C \geq 2\delta\theta$ implies $\sin\beta_C \geq \sin(2\delta\theta)$. Multiplying both sides of the last inequality by $r_1$, we get $r_1 \sin\beta_C \geq \sin(2\delta\theta)$. From (22a), we have $\Delta = r_1 \sin\beta_C$, yielding (25).

Note that $\Delta$ is related to the rotational increment in the scan $\delta\theta$. Denoting the minimum translation length by $\Delta_{min}$ and choosing $\beta_C = \arcsin(\frac{\Delta_{\min}}{r_1})$, the two curves just touch each other, as shown in Fig. 11(b). For $\Delta < \Delta_{\min}$, the two curves overlap, indicating that it is possible to make a mistake. Making $\Delta > \Delta_{\min}$, the separation between the curves increases and allows more robust differentiation.

## VII. Experimental Verification

The experimental configuration is shown in Fig. 12. A Polaroid sensor is mounted on a computer-controlled mobile robot serving as a moving platform. Custom-designed circuits are used for both the receiver and transmitter electronics. The radio-frequency echoes are digitized by an A/D converter (Motorola DSP56ADC16) operating at a 192-kHz sampling rate with 12 b of resolution interfaced to a Motorola DSP56000 signal processing board. The DSP board communicates with an IBM PC-AT, where the data are processed. The mobile vehicle is capable of computer-controlled translation and rotation. Three 400-step stepper motors are used: two to move the vehicle and the third to rotate the sensor with an incremental angle of $\delta\theta = 0.9°$. The threshold of the system was set at $\tau = 0.02A_f$ (34 dB), where the amplifier gain was set so that the maximum $A_f$ extends over the linear range of the A/D converter.

### A. Differentiation of Edges from Planes/Corners

The minimum range of detection of elements in our physical system is 7 cm, which is limited by the transient response of the transducer. From (15), (16), and (20), we get that $\delta\theta$ should be less than 4.3° for successful differentiation of edges from planes and corners. With $\delta\theta = 0.9°$, our design is conservative. Fig. 13 shows the experimentally generated sonar map of the environment. The edges are located 44 and 47 cm from the sensor. The scattering strength $\sigma_E$ for the edges was found empirically to be 0.095. For the element at 47 cm, the expected values of $\theta_{scan}$ for planes/corners and edges are determined from (15) and (16) to be 23.3 and 7.8°, respectively. Using (17), we get $b(r = 44\,\text{cm}) = \frac{23.3°+7.8°}{2} = 15.55°$. Since the observed angular extent is 7.2°, it is concluded that the element is an edge. Note that this observed value is within $\pm\delta\theta$ of the expected value of 7.8°. A similar analysis for the other edge at 44 cm shows that the observed angular extent of 8.1° is also within $\pm\delta\theta$ of the expected value of 8.0°. The observed angular extents of the plane and corner reflectors (22.5, 23.4, and 22.5°) are also within $\pm\delta\theta$ of the expected value of 23.3°.

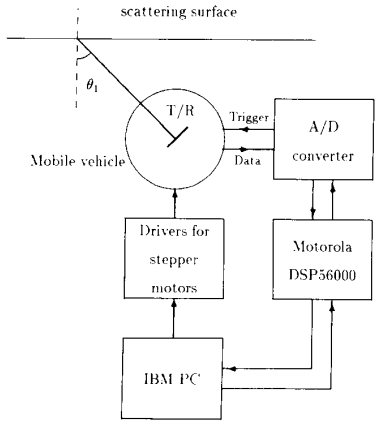


Fig. 12. Experimental setup showing the instrumentation for acquiring sonar data. The Polaroid sensor is mounted on a mobile vehicle. The reflected pulse is digitized by the Motorola DSP board interaction with the PC.

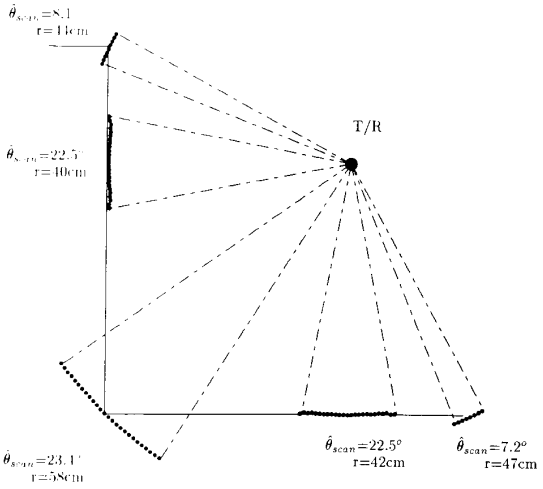


Fig. 13. Actual scan indication TOF patterns produced by a plane, corner, and an edge. Edges can be differentiated from planes and corners by their angular extents. Solid line indicates floor plan.

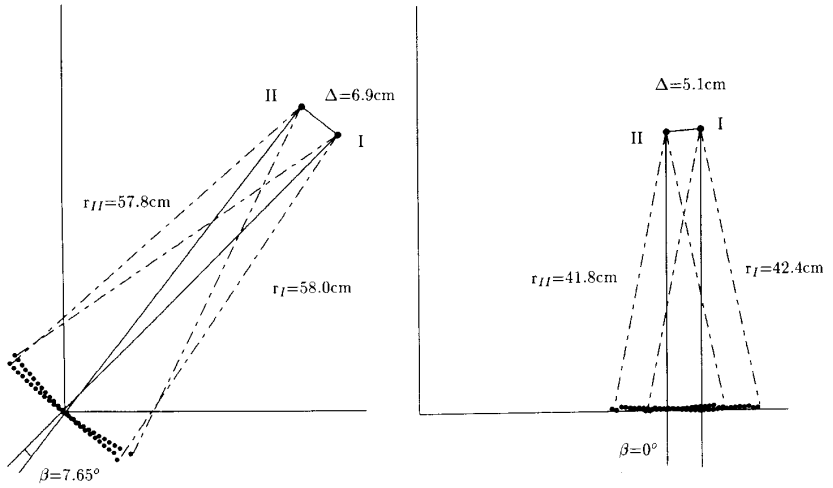


Fig. 14. Real data showing differentiation of planes and corners from the scans formed from two different locations.

### B. Differentiation of Planes from Corners

The procedure for differentiating planes and corners is demonstrated in Fig. 14 with the direction of travel chosen, as described in Seciton III-A. For the corner, $\hat{\beta}$ is equal to 7.65°. The expected value is 6.8° from (22a). Thus, the estimate is within $\pm\delta\theta$ of $\beta_C$. For the plane, $\hat{\beta} = 0°$, which is also within $\pm\delta\theta$ of $\beta_P = 0°$. Note that the translation lengths of 6.9 and 5.1 cm satisfy (25). Thus, we were able to successfully differentiate planes and corners.

## VIII. Constraints on Element Size and Interference Problems

For successful differentiation, constraints on the size of the elements in the environment need to be imposed. The constraints can be classified as follows:

**1) Minimum Size Requirements:** Objects in the real world have finite dimensions. Physical and geometrical considerations dictate two types of minimal size constraints:

**a)** In Section III, planes were defined as extensions of line segments, whereas corners and edges were defined as the intersections of planes. The minimum sizes of the constituent planes need to be determined for proper definitions of these elements.

**b)** Using a single sensor, differentiation of planes and corners requires scans from two locations. For successful differentiation, the scans from the two locations should correspond to the same element. This imposes constraints on the minimal sizes of the elements.

**2) Interference Effects:** Two types of interference are identified:

**a)** The echo in a single scan must be the result of reflection or diffraction from a single element. Overlapping echoes can result if the elements are too close to each other. An example of this type of interference is shown in Fig. 15(a).

**b)** The presence of multiple elements along the scan direction can also cause interference, as shown in Fig. 15(b).

Minimum Size: For planes and corners to be well defined (Constraint 1a)), their boundaries must extend outside the sensor beam. Otherwise, the end points cause diffracted waves that interfere with the reflected pulse from the plane or corner to be emanated. However, for practical considerations, this limit is overly conservative in the far field since the amplitude from edges is much smaller than that from planes and corners. Idealizing the sensor beam to be a cylinder of

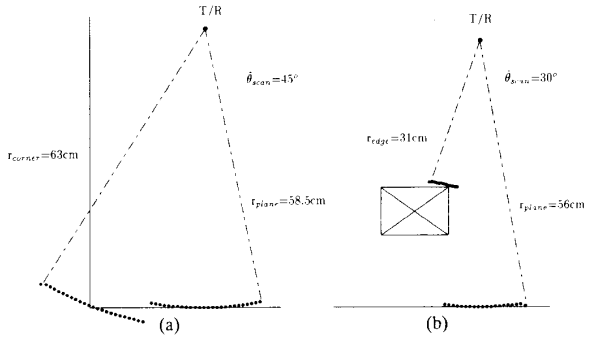


Fig. 15. Illustration of interference effects in differentiation (real data); (a) Interference is due to plane and corner elements being too close to each other; (b) presence of two elements in a single scan causes interference.

diameter equal to the aperture, we find that the parts of the plane and corner that contribute to the echo lie mostly within this cylinder [15]. Thus, the minimum dimension of a plane is the aperture diameter $2a$, as shown in Fig. 16(a). Similarly, the geometrical considerations for a corner as shown in Fig. 16(b) reveal that the minimum dimensions should be

$$(d_{C_1}, d_{C_2}) = \left(\frac{a}{\sin\alpha}, \frac{a}{\cos\alpha}\right). \tag{26}$$

To satisfy Constraint 1b) for a plane, the scan of a plane from two locations separated by $\Delta$ should correspond to the same element as shown in Fig. 17(a) or

$$\begin{aligned} d_{plane} &\geq d_{I-II} + 2a \\ &\geq \Delta\sqrt{1 - \left(\frac{\Delta}{r_I}\right)^2} + 2a \end{aligned} \tag{27}$$

where $d_{I-II}$ is the distance between the centers of the two arcs, and $a$ is the aperture radius of the sensor. Since $\Delta \ll r_I$, a reasonable approximation is

$$d_{plane} \geq \Delta + 2a.$$

If the maximum range of interest is $2m$ and a 400° stepper motor is used for the rotation of the sensor with $\delta\theta = 0.9°$, the minimum

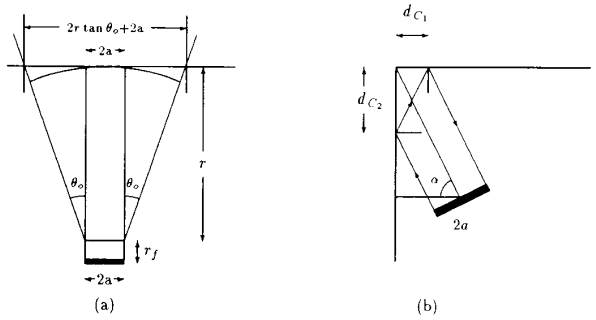


Fig. 16. Minimum size requirements: (a) For a plane, the practical minimum size is the sensor aperture 2a; (b) for a corner, the dimensions should be greater than $(d_{C_1} \times d_{C_2})$.

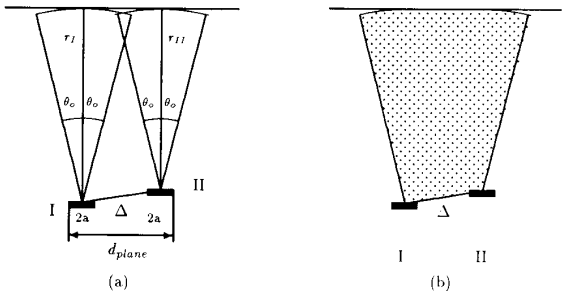


Fig. 17. Constraints for phase identification: (a) Plane should have a dimension greater than $d_{plane}$ for the proper differentiation; (b) shaded region should be void of objects for interference not to occur.

dimension for a plane must be 10 cm for successful differentiation with the Polaroid sensor from (25) and (27).

To satisfy Constraint 1b) for a corner, the dimensions of the corner should satisfy (26) for both $\theta_{N_I}$ and $\theta_{N_{II}}$.

Interference: To avoid interference, there should be no other objects within the sensor beam. For a plane, this requires that the shaded area in Fig. 17(b) be void of other objects. To analyze the possible interference in corners, let us define $\alpha$ as the orientation difference between the corner and one of its constituent planes, as shown in Fig. 18(a). Interference can occur at larger $\alpha$ values since the side plane will be very close to the corner (Fig. 15(a)). Thus, to satisfy Constraint 2a), the scan extents from the corner, and the side planes should not overlap. From the geometry of Fig. 18(a), we get

$$2\theta_o < \alpha < 90^\circ - 2\theta_o. \tag{28}$$

A combination of (28) and (26) yields

$$(d_{C_1}, d_{C_2}) \geq \left[\frac{a}{\sin(2\theta_o)}, \frac{a}{\sin(2\theta_o)}\right].$$

For the Polaroid sensor, $\theta_o = 11.8^\circ$ and $a = 1.7$ cm; thus, the minimum dimensions for a corner are [4.3, 4.3 cm]. To satisfy Constraint 2b) for corners, the shaded area in Fig. 18(b) should be void of objects.

For proper differentiation of edges, there should be no elements located close to the edge. To satisfy Constraint 2) for an edge, the shaded area in Fig. 19 should not contain any objects. Note that the angular width of this cone is $2\theta_o$, although the angular extent of the scan arc $\theta_{scan_E}$ is less than $2\theta_o$.

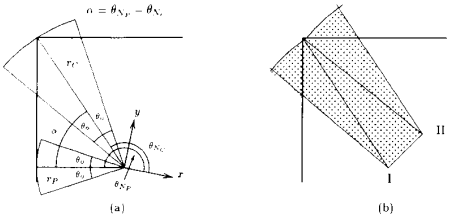


Fig. 18. (a) For interference due to the side planes not to occur $2\theta < \alpha < 90\deg - 2\theta_0$; (b) to avoid interference in the differentiation, the shaded area should be void of objects.

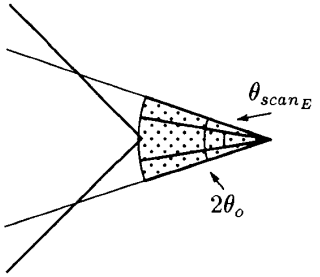


Fig. 19. Constraint on edge identification. To avoid interference, the shaded area should not contain any other element.

In typical environments, the dimensions of planes and corners are large enough for Constraints 1) and 2a) to be satisfied. However, it may be difficult to satisfy Constraint 2b) in a cluttered environment.

## IX. Discussion

The physical properties of reflection and acoustic sensors are exploited to extract information about the environment. A novel characterization of sonar data was presented that allowed the differentiation of planes, corners, and edges in a specular environment. The differentiation procedure made use of the physical properties of reflection and diffraction. Using a single mobile sensor, edges can be differentiated from planes and corners from a single location, whereas planes and corners are differentiated by scanning from two separate locations.

Limitations in differentiation arise in a cluttered environment when the elements are too close to each other. The major limitation is due to the beam width of the sensor. The resulting scan in such a case is a mixture of the echoes reflected and/or diffracted from the observed elements. However, such situations can, in most cases, be identified from the abrupt change in the range measurements.

We have neglected the effects of noise in this paper since the SNR was relatively high in our system ($\approx$ 40 dB). Note that the threshold of the system was set at 34 dB below $A_f$. The analysis can be extended to include noise. In the commonly observed case of added white Gaussian noise, the probability density functions of $\hat{\theta}_{scan}$ and $\hat{\beta}$ would not have finite extents. A confidence level criterion must then be chosen and the translation length $\Delta$ determined to allow robust differentiation.

The accuracy and performance of any sonar map building system depend heavily on the reliability of the sensor data. Using the physical properties of the reflection process and the acoustic sensors, the sensor data can be interpreted more successfully. This leads to the design and implementation of sonar systems with better performance and reliability.

## REFERENCES


[1] H. P. Moravec and A. Elfes, "High resolution maps from wide angle sonar," in *Proc. IEEE Int. Conf. Robotics Automat.*, 1985, pp. 116–121.

[2] J. L. Crowley, "Dynamic world modeling for an intelligent mobile robot using rotating ultrasonic ranging device," in *Proc. IEEE Int. Conf. Robotics Automat.*, 1985, pp. 128–135.

[3] S. Tachi and K. Komoriya, "Guide dog robot," in *Proc. Second Int. Symp. Robotics Res.* (Kyoto), 1984.

[4] G. Honderd, W. Jongkind, and C. H. van Aalst, "Sensor and navigation system for a mobile robot," in*Proc. Intell. Autonomous Syst. Conf.*, 1986, pp. 258–26.

[5] C. Jorgensen, W. Hamel, and C. Weisbin, "Autonomous robot navigation," *Byte*, pp. 223–235, Jan. 1986.

[6] D. J. Kriegman, E. Triendl, and T. O. Binford, "A mobile robot: Sensing, planning and locomotion," in *IEEE Int. Conf. Robotics Automat.*, 1987, pp. 402–408.

[7] Polaroid Corp., *Ultrasonic Ranging System HandBook*. Cambridge, MA, 1984.

[8] J. Borenstein and Y. Koren, "Obstacle avoidance with ultrasonic sensors," *IEEE J. Robotics Automat.*, pp. 213–218, Apr. 1988.

[9] R. A. Jarvis, "A perspective on range finding techniques for computer vision," *IEEE Trans. Patt. Anal. Machine Intell.*, vol. PAMI-5, pp. 122–139, Mar. 1983.

[10] G. D. Maslin, *A Simple Ultrasonic Ranging System*, presented at the 102nd Conv. Audio Eng., 1983. Reprinted in *Polaroid Ultrasonic Ranging System Handbook, Application Notes/Tech. Papers.*

[11] T. Lozano-Pérez, Foreword in *Autonomous Robot Vehicles* (I. J. Cox and G. T. Wilfong, Eds.). New York: Springer-Verlag, 1990.

[12] J. Leonard, H. Durrant-Whyte, and I. J. Cox, "Dynamic map building for an autonomous mobile robot," in*Proc. IEEE Int. Workshop Intelligent Robots Syst.*, 1990, pp. 89–96.

[13] A. Elfes, "Sonar based real-world mapping and navigation," *IEEE J. Robotics Automat.*, vol. 3, pp. 249–265, 1987.

[14] J. L. Crowley, "Navigation for an intelligent mobile robot," *IEEE J. Robotics Automat.*, pp. 31–41, Mar. 1985.

[15] R. Kuc and M. W. Siegel, "Physically based simulation model for acoustic sensor robot navigation," *IEEE Trans. Patt. Anal. Machine Intell.*, vol. PAMI-9, pp. 766–778, Nov. 1987.

[16] R. Kuc and B. Barshan, "Navigating vehicles through an unstructured environment with sonar," in*Proc. IEEE Int. Conf. Robotics Automat.*, 1989, pp. 1422–1426.

[17] M. K. Brown, "Feature extraction techniques for recognizing solid objects with an ultrasonic range sensor," *IEEE J. Robotics Automat.*, pp. 191–205, Dec. 1985.

[18] R. Kuc, "A spatial sampling criterion for sonar obstacle detection," *IEEE Trans. Patt. Anal. Machine Intell.*, vol. 12, pp. 686–690, July 1990.

[19] S. A. Walter, "The sonar ring: Obstacle detection for a mobile robot," in *Proc. IEEE Conf. Robotics Automat.*, 1987, pp. 1574–1578.

[20] Ö. Bozma and R. Kuc, "Characterizing pulses reflected from rough surfaces using ultrasound," *J. Acoustical Soc. Amer.*, vol. 89, pp. 2519–2531, June 1991.

[21] R. C. Weast, *CRC Handbook of Chemistry and Physics* (54th ed.). Cleveland: Chemical Rubber, 1973. p. E49.

[22] L. W. Camp, *Underwater Acoustics*. New York: Wiley: 1970.

[23] P. N. T. Wells, *Biomedical Ultrasonics*. New York: Academic, 1977, pp. 26–31, ch. 2.

[24] A. D. Pierce, *Acoustics: An Introduction to Its Physical Principles and Applications*. New York: McGraw-Hill, 1981.

[25] B. Barshan and R. Kuc, "Differentiating sonar reflections from corners and planes by employing an intelligent sensor," *IEEE J. Patt. Anal. Machine Intell.*, vol. 12, pp. 560–569, June 1990.

[26] J. J. Craig, *Introduction to Robotics: Mechanics and Control*. Reading, MA: Addison-Wesley, 1986.

[27] J. B. Keller, "Geometrical theory of diffraction," *J. Opt. Soc. Amer.*, vol. 52, pp. 116–130, Feb. 1961.

[28] P. M. Morse and K. U. Ingard, *Theoretical Acoustics*.New York: McGraw-Hill, 1968.

[29] R. Kuc and V. B. Viard, "A physically based navigation strategy for sonar-guided vehicles," *Int. J. Robotics Res.*, vol. 10, pp. 75–87, Apr. 1991.

[30] N. S. Tzannes, *Communication and Radar Systems* Englewood Cliffs, NJ: Prentice-Hall, 1985, pp. 111–113.

[31] A. Papoulis, *Probability, Random Variables and Stochastic Processes*. New York: McGraw-Hill, 1965; 2nd ed., 1984.